Remote Sensing of Environment 210 (2018) 422–433

Contents lists available at ScienceDirect

Remote Sensing of Environment

journal homepage: www.elsevier.com/locate/rse

Drivers of spatial variability in greendown within an oak-hickory forest landscape

V.C. Reaves[a,*], A.J. Elmore[a], D.M. Nelson[a], B.E. McNeil[b]

[a] University of Maryland Center for Environmental Science, Appalachian Laboratory, 301 Braddock Road, Frostburg, MD 21532, USA
[b] Department of Geology and Geography, 98 Beechurst Avenue, 330 Brooks Hall, Morgantown, WV 26506-6300, USA

ARTICLE INFO

Keywords:
Phenology
Landsat
Temperate deciduous forest
Canopy structure
Plant traits

ABSTRACT

Declining near-infrared (NIR) surface reflectance between early and late summer, here termed greendown, is a common, yet poorly understood phenomena in remote sensing time series of temperate deciduous forests. As revealed by phenology analysis of Landsat satellite data, there are strong spatial patterns in the rate of greendown across temperate deciduous forest landscapes, and analyzing these patterns could help advance our understanding of surface reflectance drivers. Within an oak-hickory (*Quercus* spp. – *Carya* spp.) forest landscape in western Maryland, USA, we tested how spatial patterns in greendown related to potential drivers at the landscape-, tree crown- and leaf-levels. We found that 50% of the spatial variability in greendown was explained by landscape variables, with greendown particularly higher in locations with higher maximum greenness, more southerly aspects, or locations with greater abundance of white oak (*Quercus alba*). The importance of species composition as a driver of greendown was supported at the tree crown level, where, relative to three other tree species, white oak exhibited the most consistent trend toward more vertical leaf angles later in the season. At the leaf level, NIR reflectance decreased in productive sites where %N increased, and $\delta^{13}C$ decreased, through the season. However, among all sites, there were no consistent seasonal trends in foliar NIR reflectance, and we found no correlation among leaf-level NIR reflectance and satellite-observed greendown. Collectively, these results suggest that the spatial variability of greendown in this oak-hickory forest is most strongly controlled by an interaction of topographic and species compositional drivers operating at the landscape and tree crown levels. We found spatial analysis of greendown to be a useful approach to explore landscape-, tree crown-, and leaf-level controls on surface reflectance, and thereby help translate land surface phenology data into predictions of ecosystem structure and functioning.

1. Introduction

The annual trajectory of spectral reflectance observed in remote sensing data is used to infer many aspects of ecosystem structure and functioning, including land use, forest disturbance, and productivity (Fisher et al., 2006; Elmore et al., 2012; Zhu and Woodcock, 2012; Zhu and Woodcock, 2014; Badgley et al., 2017). As data from medium resolution sensors have become more widely and freely available (Woodcock et al., 2008), these data have been leveraged to describe ever more complex and variable phenomena. This is particularly true when characterizing land surface phenology patterns over space and time (Melaas et al., 2012; Melaas et al., 2016). For instance, one common, but poorly understood, intra-annual phenomenon is declining near-infrared reflectance (NIR) through the growing season in broadleaf deciduous forest canopies, which we call “greendown”. Greendown has been observed in data collected by different observation platforms at varying spatial scales, including from tower-based webcams (Elmore et al., 2012; Keenan et al., 2014), from dense stacks of Landsat data organized by day of year (Fisher et al., 2006; Elmore et al., 2012; Melaas et al., 2013), and MODIS phenology products (Zhang et al., 2004; Fisher et al., 2006). Thus, greendown appears to be a common phenological feature of spectral reflectance time series, yet little work has attempted to link spatial patterns of greendown with forest structure or function.

At landscape scales, greendown could be related to abiotic mechanisms related to changing sun-sensor-canopy geometry through the growing season, especially the interaction of a changing sun angle, topography, and canopy structure. Although many common pre-processing algorithms correct satellite reflectance data for these changes in sun-sensor-topography geometry (i.e. Gu and Gillespie, 1998), the physical structure of the canopy itself is not commonly accounted for, and could interact with topography to affect reflectance. Specifically,

* Corresponding author.
E-mail address: vmlcunningham@gmail.com (V.C. Reaves).

https://doi.org/10.1016/j.rse.2018.03.027
Received 1 August 2017; Received in revised form 17 March 2018; Accepted 19 March 2018

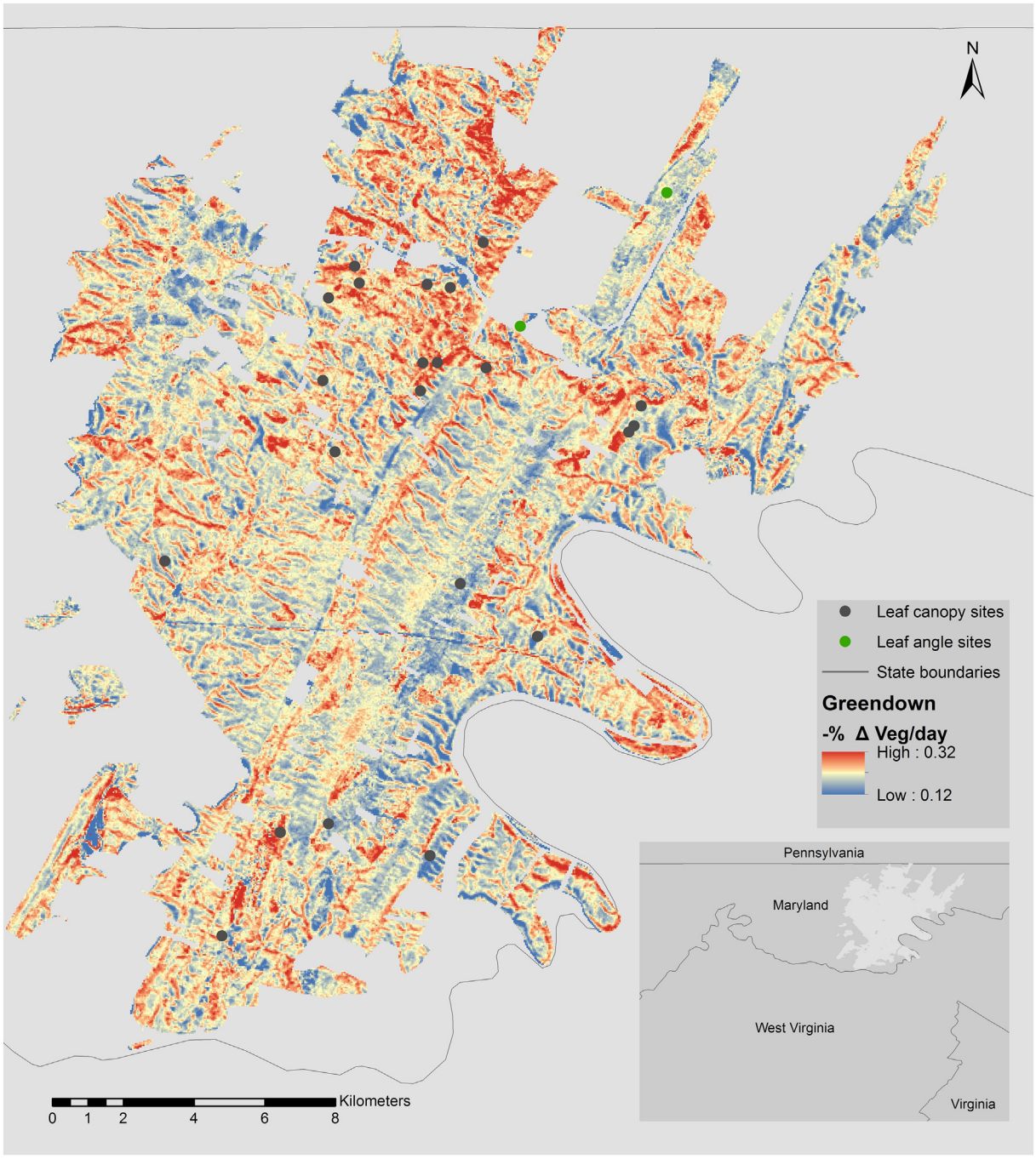

Fig. 1. Map of study area at Green Ridge State Forest. Leaf collection sites (black circles), leaf angle sites (green circles), are overlaid on greendown values (color scale). The greendown scale excludes the highest and lowest 2% of its range which were values not typical of interior forest but rather of open landscapes. (For interpretation of the references to color in this figure legend, the reader is referred to the web version of this article.)

forest stands on different slope aspects experience different light and moisture availability, which can influence canopy structure through changes in tree species composition. Owing to variation in crown architecture between tree species, such as variation in crown shape, density, and leaf angle distribution (Ollinger, 2011), canopies can exhibit variation in shading within and between tree crowns (Asner and Warner, 2003). Thus, the top-of-canopy complexity, or rugosity induced by the mix of species with varying architectures could interact with the seasonal sun angle changes to affect spatial patterns of greendown (Parker and Russ, 2004; Ogunjemiyo et al., 2005).

Leaf angle distribution of forest trees is another important determinant of spectral reflectance (Asner, 1998) and can vary among species, locations, and through the growing season (Pisek et al., 2013; Raabe et al., 2015). Leaf angle influences NIR reflectance by modifying the apparent leaf area as observed from nadir (Asner, 1998). While leaf angle varies characteristically between species, trees may also modify leaf angle in response to changes in environmental conditions, thus representing an adaptive, biotic mechanism by which trees dynamically adjust leaf exposure to sunlight. Especially for anisohydric species that keep their stomata open, even during periods of late-summer drought (Choat et al., 2012; Roman et al., 2015), increasing leaf angle (i.e., more vertical leaf angles) is likely related to reduced evapotranspirative water loss. An empirical link between increasing leaf angle and greendown would therefore suggest that greendown indexes species

water use strategies.

At the level of individual leaves, foliar spectral reflectance can exhibit variability that does not closely match the trajectory of canopy development and spectral reflectance (Yang et al., 2014). For example, while canopy greenness from web cameras has been shown to reach a maximum about two weeks after the onset of greenness, foliar NIR reflectance and leaf chemical traits continue to increase for another two weeks before declining gradually throughout the remainder of the growing season (Keenan et al., 2014; Yang et al., 2014). Therefore, although observations of declining surface reflectance through the growing season could be related to changes in foliar reflectance, current observational data do not fully support this idea. However, spatial variation in the temporal patterns of foliar traits and foliar reflectance has not been extensively investigated (Keenan et al., 2014). Although variation between sites has been observed (i.e. (Yang et al., 2016)), there remains a need to characterize how growing season trends in foliar traits and foliar reflectance vary across landscapes. When paired with pertinent environmental data, such a perspective has the potential to reveal changes in forest functioning throughout the growing season (Elmore et al., 2012), such as water use strategies or gradients in productivity.

Landscape, tree crown- and leaf-level mechanisms could synergistically cause the occurrence of greendown through combining abiotic (topography) and biotic (species assemblage, leaf angle, foliar reflectance) drivers. Identifying the factor(s) controlling greendown is important because it could lead to a new understanding of how forest ecosystems respond to environmental change across space and time, as well as suggest new methods for mapping functional attributes of forests. For instance, understanding the relationship between topographic variables and greendown may provide insight into medium-scale variability in forest functioning and forest responses to important drivers related to climate change (Zhang et al., 2003; Zhang et al., 2004; Fisher et al., 2006; Hwang et al., 2011; Dragoni and Rahman, 2012; Hwang et al., 2014; Keenan et al., 2014). Here, we use a combination of remote and field-based observations to investigate the degree to which landscape-, tree crown-, and leaf-level observations explain spatial variability in greendown at Green Ridge State Forest, a temperate deciduous forest in the mid-Atlantic region of the United States.

2. Methods

2.1. Study area

This study was conducted in Green Ridge State Forest (GRSF), located in the Ridge and Valley physiographic province in Allegany County, western Maryland (Fig. 1). Two major northeast-southwest orientated ridges run through the middle of the forest. Elevation ranges from 152 m to 610 m. Mean annual temperature is 12 °C and mean annual precipitation is 94 cm (Owenby and Ezell, 1992). Most of the forest at GRSF was harvested for timber by the early 1900s. Today GRSF is a mixed oak forest of diverse age resulting from mostly small stand forest harvests since the 1960s. The forest is owned and operated by Maryland Department of Natural Resources Forest Service with the exception of private inholdings (gray areas within park boundaries in Fig. 1). Dominant forest tree species are oaks (*Quercus alba*, *Q. rubra*, *Q. coccinea*, *Q. prinus*, *Q. velutina*) and hickory (*Carya glabra*, *C. tomentosa*) with occasional stands of pine (*Pinus strobus*, *P. rigida*, *P. virginiana*).

2.2. Landsat data processing

From the USGS, we acquired Landsat Ecosystem Disturbance Acquisition Processing System (LEDAPS) (Masek et al., 2006) surface reflectance data for all available Landsat TM and ETM+ scenes in path 16/row 33, spanning years 1982–2013. LEDAPS processing also generates cloud/cloud shadow masks, which were used to identify clear, high quality pixel observations, resulting in an average of 182 ± 5 (1SD) observations per location. We applied a sun-canopy-sensor correction to normalize for first order topographic effects and differences in sun zenith angle among images (Gu and Gillespie, 1998). The correction employed reduces the difference in radiance measured from topographic positions with more or less solar exposure. This technique has been used to normalize for topography while emphasizing actual structural differences in forests, such as those due to forest harvest history (Sabol et al., 2002). However, neither the LEDAPS processing nor the sun-canopy-sensor correction adjusts for changes in the bidirectional reflectance distribution function (BRDF) throughout the growing season. In a post-hoc analysis, we evaluated greendown before and after the sun-canopy-sensor correction and found that it had no consistent effect on greendown, neither consistently increasing or decreasing the decline in growing season NIR reflectance. To each image, we applied linear spectral mixture analysis (SMA) (Adams et al., 1986; Smith et al., 1990; Elmore et al., 2000), which decomposed multispectral surface reflectance into the fractional abundance of four endmember spectra (photosynthetic vegetation, non-photosynthetic vegetation, substrate, and shade). Endmember spectra were identified by evaluating the spectral mixing space across all available Landsat scenes and choosing image spectra that matched the intended surface types and also occupied the outer edges of the mixing space (Small, 2004). The fraction of photosynthetic vegetation (f_{pv}) as calculated through SMA represents a 30+ year record, with roughly 5 to 10 observations each year. We organized these data by day of year to form a time series of f_{pv} that represents the average annual trajectory of f_{pv} through spring, summer, and autumn.

2.3. Fitting phenology curve

Here we calculate greendown from vegetation cover measurements derived using SMA of Landsat data. Landsat surface reflectance observations confirm that the decline in vegetation cover observed through the growing season is driven by declining NIR reflectance, while reflectance in the visible wavelengths is relatively stable through this period (Fig. 2). Therefore, greendown could conceptually be calculated from NIR reflectance alone or from any vegetation index sensitive to the contrast between NIR and visible reflectance. Spectral mixture analysis, however, provides a robust measure of vegetation cover that exhibits reduced sensitivity to snow cover in the spring (Fisher et al., 2006) and is more accurate than NDVI as a measure of vegetation change (Elmore et al., 2000). After measuring f_{pv}, we used the greendown-phenology model developed by Elmore et al. (2012) to derive average phenology curves fit to all available Landsat observations of f_{pv} (Eq. (1)), organized by day of year, for all pixels.

$$f_{pv}(t, \mathbf{m}) = m_1 + (m_2 - m_7 \cdot t)\left(\frac{1}{1 + e^{(m3-t)/m4}} - \frac{1}{1 + e^{(m5-t)/m6}}\right) \quad (1)$$

The left side of Eq. (1) is the photosynthetic vegetation fraction observed on any day of year (t) in the Landsat record. The model parameters, $\mathbf{m} = [m_1, m_2, m_3, m_4, m_5, m_6, m_7]$ control the shape of the phenology curve fit to these observations, where m_1 is the minimum vegetation cover; m_2 is the potential amplitude between m_1 related to the maximum vegetation fraction. Greendown is m_7, which indicates the rate of decline in vegetation cover during the growing season. Parameters m_3 and m_5 are the day of year when greenness is most rapidly changing (inflection points) in spring and autumn. Parameters m_4 and m_6 arc proportional to the number of days f_{pv} takes to increase or decrease during the spring and autumn transitions, respectively. We fit Eq. (1) to all pixel locations at GRSF using inverse methods that aim to fit the curve to the median f_{pv} on each DOY (i.e., L1 normalization, a method to optimize a model by minimizing the absolute value of model residuals) (Scales et al., 1988; Farquharson and Oldenburg, 1998) thus reducing the importance of outlier f_{pv} observations (Elmore et al., 2012). From the result of this fit to the data we extracted each of the model parameters and also numerically calculated maximum

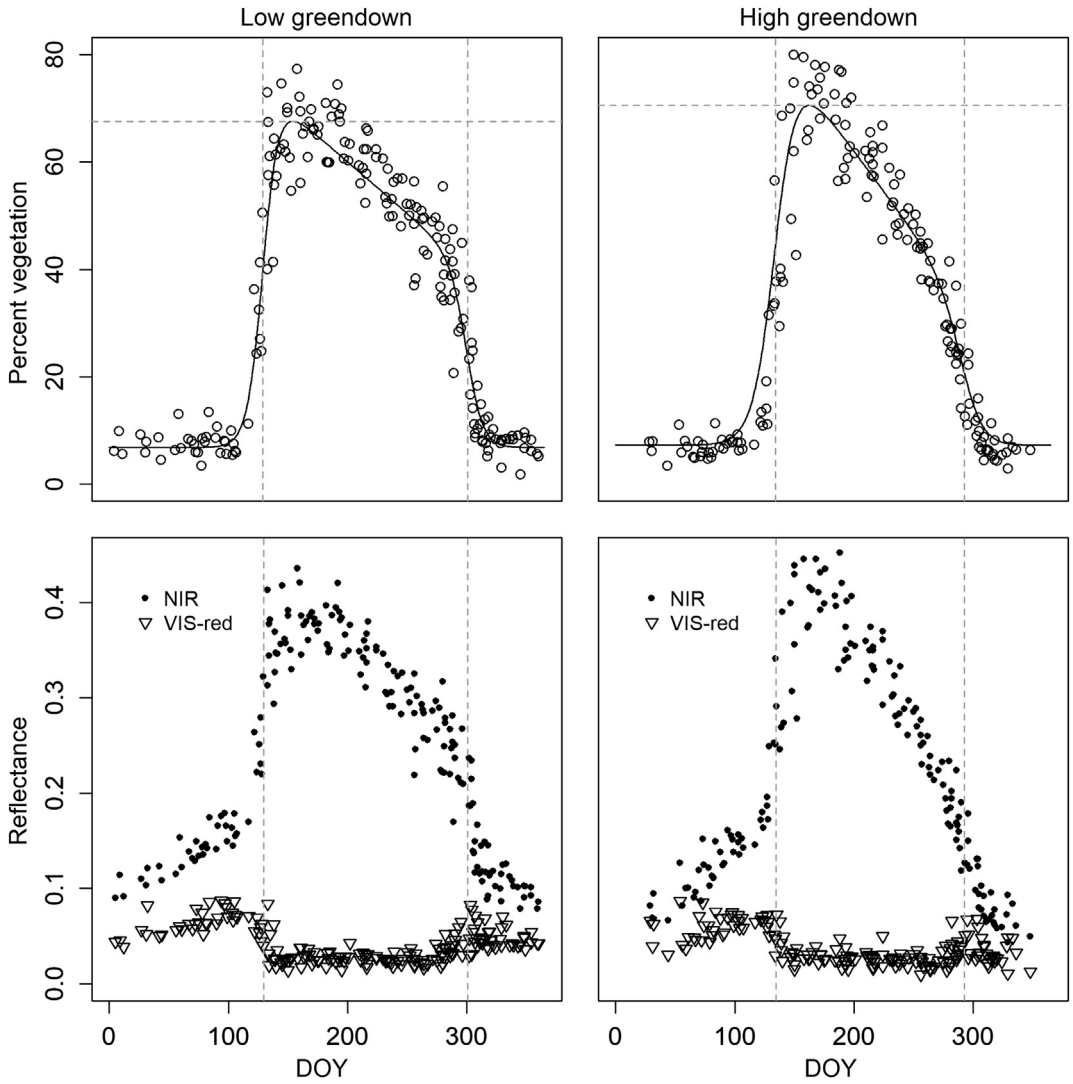

Fig. 2. Examples of the greendown-phenology curve for two pixels at Green Ridge State Forest, Maryland, USA, low greendown (left), high greendown (right). Each point represents a single pixel observation of vegetation cover (upper panels; calculated using spectral mixture analysis) or surface reflectance (lower panels) from Landsat, and the solid black line is the fitted greendown-phenology model. The vertical gray dotted lines indicate the inflection points in spring and autumn. In these examples, the spring and autumn inflection points occurred on DOY 130 and 301 for low greendown, and DOY 135 and 293 for high greendown, respectively. The horizontal gray dotted line indicates mean maximum vegetation. Greendown is the slope of the line following maximum vegetation cover.

vegetation (MaxVeg), as the maximum of Eq. (1). Elmore et al. (2012) calculated 95% uncertainty values for each parameter in Eq. (1) using bootstrap resampling with 5000 iterations and arrived at a greendown (m_7) uncertainty of ± 0.0007 f_{pv} day^{-1}. We rescaled greendown by multiplying it by 100 to arrive at units of percent f_{pv} decline per day. Negative values of m_7 are extremely rare (1% of GRSF), but represent locations where f_{pv} increased throughout the growing season. Likewise, extreme positive values (> 0.6) were < 1% of GRSF. Pixels at the extreme ends of the greendown range were confined to agriculture fields and barren lands and were thus excluded from further analysis. We verified interior forest coverage of the Landsat pixels with recent high resolution orthophotos available from the National Agricultural Imagery Program.

2.4. Geospatial data

To map the ground surface and outer tree canopy topography at GRSF, we acquired leaf-off LiDAR data from an aerial survey that the Allegany County, Maryland planning office conducted on January 29 and 31, 2012, and February 03, 2012. The return density for the LiDAR data depended on vegetation complexity, but ranged from 1–4 pts/m^2. Using standard techniques (US Forest Service Fusion software version 3.41), we generated a 2-m digital elevation model (DEM), canopy height model (CHM) and canopy surface model (canopy height + elevation). We calculated slope and aspect from the 2-m DEM using eight cell neighbors, and folded aspect as degrees relative to north (0 = north, 180 = south, 90 = east or west). We used the 2-m canopy surface model and the ArcGIS solar analysis tool to calculate total solar irradiance. We aggregated cells from each of these 2-m resolution products to a Landsat resolution (30-m resolution pixel), using mean values of slope, elevation, aspect, and solar irradiance, and maximum values for canopy height. To summarize the complexity of the outer-canopy surface, we calculated canopy rugosity as the standard deviation of canopy height from all 2-m canopy height observations within the area of each Landsat pixel footprint.

To obtain vegetation type (alliance level) for all landscape points, we used a species composition map of GRSF developed by Foster and Townsend (2004) from 17-m resolution airborne AVIRIS imaging spectrometer data. Alliance level tree associations classify tree stands based on the dominant or co-dominant tree species (Jennings et al., 2009). The map developed by Foster and Townsend (2004) identified 28 forest associations at GRSF, 21 of which were captured in our more

narrowly defined study area.

2.5. Site selection

We sampled the study area using three sets of study sites. For the first set, we selected 1000 random points that fell within interior forest at GRSF. At these locations, we sampled each of the geospatial data products described previously, including the Landsat-derived phenology parameters (i.e., parameters m_1 through m_7). We found that 60 of the points fell on pixels covering mixed landcover (i.e., managed open space, open water, roads, etc.) so we removed these points from the site list to arrive at a final selection of 940 forested sites.

For our second set of sites, we used the parameters from the greendown phenology model and maps of rugosity derived from LiDAR to identify a suite of 21 stratified random locations for foliar sampling. First, we classified greendown into four categories that spanned its range. We then classified rugosity as either low, medium or high. Finally, we intersected this classification with the greendown classification resulting in 12 classes representing the full range and all combinations of rugosity and greendown. Within each class, we excluded areas that were $< 1000\ m^2$ to eliminate the possibility of establishing sites in heterogeneous areas where the chance of sampling the wrong greendown or rugosity class was largest. We used a random point generator to identify an equal number of locations in each stratified class, and chose points for sampling based on accessibility and the presence of the target species (*Q. alba*, as discussed below). This resulted in a total of 21 sites within the 12 greendown classes with an average of 2 sites per class, 10 characterized by high rugosity and five by low rugosity.

The third set of sites (two sites) were selected based on access and ability to collect repeat photographs for leaf angle measurements. For these measurements, a photographer is required to be level with the sunlit upper crowns of mature (~100 years old) trees within a closed-canopy forest, which is a unique requirement limiting the number of locations available. These sites were separate from the 21 sites that *Q. alba* leaves were collected because access to take canopy level photographs were not available at the 21 sites. One of the leaf angle sites was from an overlook platform that extended out from a steep slope behind the GRSF visitor center, where pictures of the sunlit upper crown-level of downslope white oak (*Q. alba)* trees were taken. The second site was an abandoned fire tower that was surrounded by mature *Q. velutina*, *Q. prinus* and *C. tomentosa* trees.

2.6. Leaf collection

At each of the 21 sites established for foliar analyses, we collected sunlit leaves from *Q. alba* in early and late summer of 2014. We focused on *Q. alba* because (1) it is commonly found throughout GRSF as a dominate species in the upper canopy and was likely to be found throughout the full range of greendown values, and (2) by constraining our analysis to a single species we intended to control for potential inter-specific variation in leaf-level variables (i.e. N concentration and reflectance values). All sites had three *Q. alba* trees present in the upper canopy with the exception of one site which had only one large *Q. alba* located in a dominantly *Liriodendron tulipifera* stand. The date of early summer sampling for each site was in mid-June, approximately 4 weeks after spring onset DOY (m_3; Eq. (1)). This timing meant that sites were exhibiting the same pheno-phase during the first sampling. Similarly, for the late summer sampling in late August, sampling occurred on average 58 days before autumn offset (m_5; Eq. (1)) to avoid collecting leaves during the period of rapid senescence. We selected a subset of four sites (out of the 21) for three additional samplings in two-week intervals between the early and late summer sample collections.

We collected leaf samples using a 12-gauge shotgun with a modified choke and #4 steel shot in 2 ¾" shells with a 1½ oz load. The gun operator aimed for a small twig that had a cluster of leaves at the top of the tree crown. On each of the sampled trees, we collected separate twigs from different sides of the crown to account for within-crown variation. For each retrieved twig, we kept leaves hydrated by either: (1) wrapping the base of the twig in a wet paper towel and placing it in a re-closable plastic bag, or (2) placing the twig base in a floral water tube. We stored all leaf samples in a cooler until we processed them at the lab within five hours of sample collection. We selected one leaf from each twig for analysis. This process yielded 122 leaf samples for each of the early and late summer collection periods. From the subset of 4 plots sampled every two weeks between early and late summer, each collection yielded between 45 and 48 samples.

2.7. Spectral measurements

We measured fresh leaf spectra using an Analytical Spectral Devices Inc. (ASD; Boulder, CO, Fieldspec Pro FR spectrometer (350–2500 nm range). An area of the leaf that was at least 2-cm in diameter and had the least amount of visible imperfections was chosen for the spectral measurement. Spectral measurements were taken three times and averaged for each measured leaf sample. Viewspec Pro version 4.05 was used to post-process the spectra, including a splice correction to account for gain differences between the first and second detector. To maximize comparability with Landsat observations we calculated broad-band reflectance in two wavelength regions: VIS-red (band 3, 0.63–0.69 mm) and NIR (band 4, 0.77–0.90 mm). We used VIS-red and NIR broad-band reflectance measurements to calculate the normalized difference vegetation index (NDVI), a widely used remote sensing index for greenness (photosynthetic capacity) (Tucker, 1979).

2.8. Leaf traits and isotope analysis

We measured foliar $\delta^{13}C$ and nitrogen concentration (%N) to track changes in leaf chemical traits throughout the growing season. Leaf $\delta^{13}C$ values indicate the degree to which a plant discriminates against ^{13}C during photosynthesis, which is a function of the ratio of intercellular to atmospheric CO_2 concentrations resulting from changes in photosynthesis and/or stomatal conductance (i.e. intrinsic water use efficiency, iWUE). Likewise, foliar %N has been used as a proxy for productivity due to its role in photosynthesis (Reich et al., 1991; Wilson et al., 2000). For each sampled leaf, we punched out a 2-cm diameter leaf section (the same section that was used to acquire a reflectance spectra), dried it at 60 °C for 48 h, and then ground it to a powder using a Qiagen TissueLyser II. We measured $\delta^{13}C$ and %N values of the leaf powder using a Carlo Erba NC2500 elemental analyzer (CE Instruments, Milan, Italy) interfaced with a ThermoFinnigan Delta V+ isotope ratio mass spectrometer (IRMS; ThermoFisher Scientific, Bremen, Germany) at the Central Appalachians Stable Isotope Facility (CASIF) located at the Appalachian Laboratory. We normalized leaf $\delta^{13}C$ values to VPDB using a two-point normalization curve with internal leaf standards calibrated against USGS40 and USGS41. As determined by an internal leaf standard analyzed alongside the samples, analytical precision (1σ) was 0.28‰ for $\delta^{13}C$ and 0.2% for %N.

2.9. Leaf angle

Photographs were taken in the beginning of June, July and August of 2015 to measure leaf angle using the level digital camera method (Ryu et al., 2010; Pisek et al., 2011). For each of the four species photographed (*Q. alba*, *Q. velutina*, *Q. prinus* and *C. tomentosa*), leaf angle was measured by selecting photographed leaves whose top surface was approximately perpendicular to the viewing angle of the digital camera, and measuring the angle between the leaf surface normal and zenith. Therefore, horizontally positioned leaves have a leaf angle of zero and leaves angled downward from horizontal have leaf angles > 0° to a maximum of 90 degrees (leaves hanging straight down).

2.10. Statistical analysis

All statistical analyses were completed in the R statistical environment (version 3.1.2). To evaluate effects of landscape-level variation in greendown, we developed a linear model with model effects of maximum vegetation (MaxVeg), elevation, slope, aspect, rugosity, vegetation type, and solar irradiance. To test the sensitivity of the model to each effect, we developed seven subsequent models that iteratively removed one model effect (models 2–8). We performed an ANOVA on all models to determine percent sum squared variance explained by each model effect. The percent sum of squared variance explained by each model effect was calculated by dividing the sum of squared variance for each effect by the total sum of squared variance, times 100. We used the Akaike Information Criterion (AIC) to facilitate model comparison.

To analyze for change between the early and late summer leaf sampling periods in June and August, we calculated delta (Δ) as the August – June difference for mean leaf values for each leaf variable (i.e., Δ-VIS-red). Thus, positive Δ values indicate an increase from June to August. We calculated the Pearson correlation among greendown and Δ-VIS-red, Δ-NIR, Δ-NDVI, Δ-δ^{13}C and Δ-%N. A dependent *t*-test was performed to test for differences between June and August means in all leaf variables. To explore variability in the data, we also averaged leaf-level measurements to the tree level and plotted them alongside site-level data. For the analysis of leaf angle, we used a one-way ANOVA with leaf angle as the response variable and sampling date as the model effect, thus testing for differences between leaf angle among the three different dates for each of the four tree species measured. A Tukey post hoc test was performed to determine which paired observation dates differed.

3. Results

3.1. Landscape-level drivers of greendown

Among the eight models tested, R^2 values ranged from 0.43 (the model excluding MaxVeg) to 0.50 (model with all variables, and models excluding slope or rugosity). MaxVeg explained 20–26% of variance in greendown (Table 1), with higher MaxVeg correlated to higher greendown (Table 2). Vegetation type was typically the second most explanatory variable, accounting for 8–12% of greendown variance. Vegetation class was significant in all models where it was included (Table 1). Among the 21 vegetation classes, *Quercus alba* class had a highly significant positive correlation with greendown ($p < 0.001$), except in the model that excluded MaxVeg (Table 3). The *Tilia americana- Acer saccharum* vegetation class was the only other class that was also significantly positively correlated with greendown ($p < 0.01$). In the model that excluded MaxVeg, evergreen vegetation classes (i.e., *Pinus virginiana*, *Pinus strobus*) were significantly negatively correlated with greendown ($p < 0.01$).

Aspect explained 7–10% of greendown variance, with more southerly aspects correlated with higher greendown. Lower elevations also were correlated with higher greendown, and elevation explained 5–8% of greendown variance in models including aspect and MaxVeg, but < 4% in models excluding these variables. Slope never explained more than 1% of greendown variance but this significant relationship indicated that steeper slopes were correlated with higher greendown ($p = 0.004$). Solar irradiance explained 2–4% of greendown variance across all models with more sunlit locations correlated with higher greendown. Finally, locations with lower canopy rugosity were correlated with higher greendown; rugosity explained < 1% of variance in greendown ($p = 0.01$). AIC revealed that the model that included all explanatory variables had the best goodness of fit followed by the model excluding rugosity. The AIC weight (w_i) gave the model with all variables an 88.1% probability of being the best model among all eight models.

3.2. Tree crown-level drivers of greendown

The mean leaf angle for *Q. alba* increased from June to August (50.98°, 59.91°, 69.54°) sampling dates (Fig. 3). Mean leaf angle for *Q. prinus* (54.30°, 66.95°, 68.18°) and *Q. velutina* (51.73°, 59.88°, 62.02°) increased between June and July, but there was no difference between July and August. Mean leaf angle for *C. tomentosa* (61.80°, 68.79°, 58.65°) increased between June and July and decreased between July and August, with no difference between June and August.

3.3. Leaf-level drivers of greendown

Averaged to the tree level, foliar %N ranged from 1.2 to 2.4% in June and August. Averaged to the site level, a *t*-test revealed that foliar %N did not change between June (mean value of 1.9%) and August (mean value of 1.8%, $p = 0.4$, Table 4A). However, June foliar %N was negatively related to Δ %N, indicating that sites with higher foliar %N in June had larger declines in foliar %N through the season ($R^2 = 0.19$; $p = 0.026$). Foliar δ^{13}C ranged from −28.7 to −31.9‰ at the tree-level, and site-level averages did not change between June and August (Table 4A). However, like for foliar %N, sites with higher δ^{13}C values in June experienced a larger decline in δ^{13}C by August ($R^2 = 0.54$; $p < 0.001$).

Although there was a significant increase in foliar VIS-red reflectance that contributed to a decrease in foliar NDVI between June and August, foliar NIR reflectance did not differ between the June and August sampling periods (Table 4A). Nevertheless, larger decreases in

Table 1
Greendown variance explained by each explanatory variable, modeled R^2 and AIC for each linear model. Dashed line (–) indicates model effect was excluded from the model. AIC weight (w_i) is the percent probability of goodness of fit among all the models tested. Bold indicates significance ($p < 0.05$) for modeled sum squared variance.

Explanatory variables	Units	% sum squared variance explained							
		Model 1	Model 2	Model 3	Model 4	Model 5	Model 6	Model 7	Model 8
Intercept	% Δ Veg d^{-1}	**2.44**	**0.58**	**3.34**	**2.14**	**4.88**	**2.35**	**2.09**	**21.29**
MaxVeg	% Veg	**23.31**	**22.70**	**22.55**	**23.13**	**25.89**	**23.58**	**20.04**	–
Elevation	m	**4.56**	**5.87**	**4.77**	**4.78**	**7.84**	**3.91**	–	**1.47**
Aspect	Degree	**8.01**	**9.57**	**7.93**	**8.49**	**7.19**	–	**7.27**	**6.97**
Vegetation type	–	**7.88**	**8.16**	**7.99**	**7.93**	–	**7.91**	**12.00**	**11.14**
Rugosity	Std (m)	**0.36**	**0.54**	**0.41**	–	**0.42**	**0.89**	**0.61**	**0.31**
Slope	°	**0.46**	**0.92**	–	**0.51**	**0.62**	**0.51**	**0.74**	**0.07**
Solar irradiance	WH/m^2	**2.49**	–	**2.92**	**2.66**	**2.58**	**4.15**	**3.83**	1.89
R^2	–	0.50	0.48	0.47	0.50	0.49	0.43	0.47	0.43
AIC	–	−3979.88	−3936.68	−3973.36	−3975.21	−3883.63	−3843.47	−3900.62	−3625.14
w_i	–	88.10%	0.00%	3.37%	8.53%	0.00%	0.00%	0.00%	0.00%

Table 2
Model results relating all landscape variables to greendown.

Explanatory variables	Units	% sum of squared variance explained	Estimates	p-value
Intercept	% Δ Veg d^{-1}	2.44	0.1317 ± 0.01985	< 0.001
MaxVeg	% Veg	23.31	0.3145 ± 0.01532	< 0.001
Elevation	m	4.56	−0.0001581 ± 0.00001741	< 0.001
Aspect	Degree	8.01	−0.0002676 ± 0.00002224	< 0.001
Vegetation type*	–	7.88	–	–
Rugosity	Std (m)	0.36	−0.002254 ± 0.0008841	0.0109
Slope	°	0.46	0.0004178 ± 0.0001449	0.0040
Solar irradiance	WH/m^2	2.49	−0.0000002346 ± 0.00000003498	< 0.001

* Estimates and p-values for vegetation type can be found in Table 3.

NIR reflectance between June and August (i.e. larger negative values of Δ-NIR) were related to larger decreases in foliar $\delta^{13}C$ and larger increases in foliar %N (Fig. 4). Despite these relationships between growing season changes in foliar chemical traits and foliar reflectance, there was no correlation between Landsat greendown and change in any of the measured foliar reflectance variables (Δ-VIS-red, Δ-NIR, Δ-NDVI) (Fig. 5; Table 4B). Further, there was no correlation between greendown and the change in either of the foliar chemical traits ($p = 0.18$ for %N and $p = 0.33$ for $\delta^{13}C$, Table 4B). There were no consistent temporal trends of $\delta^{13}C$, %N, NIR or VIS-red from the four intensively sampled sites throughout the growing season, supporting observations made at the full set of 21 sites (Fig. 6).

4. Discussion

4.1. Landscape-level variables

The interactive effects of topography and species composition explained roughly half of the spatial variability in greendown. Topographic position (elevation and aspect relative to north) influences energy and moisture balance in forests (Perry, 1994) and therefore would be expected to spatially correlate with edaphic factors related to resource availability and vegetation type. These landscape variables interact because tree species differ in their ability to maintain photosynthetic capacity throughout the growing season (Bassow and Bazzaz, 1998), which might directly influence greendown, or alternatively contribute to the establishment of species turnover across landscapes. Resource availability to our focal species *Q. alba*, as indexed by foliar $\delta^{13}C$ and %N, was not a significant effect on greendown (see leaf-level variables section below). Therefore, if resource availability is related to greendown in this ecosystem, we suspect it is through its control on plant community processes that influence the spatial pattern of vegetation type.

Our results comparing greendown across vegetation associations support the idea that topographic factors indirectly influence greendown through vegetation type, which explained 8–12% of model variance. For example, a study in the central Appalachian mountains found that *Q. alba*, *Q. velutina* and *Nyssa sylvatica* had a preference for southwest facing aspects whereas *Acer saccharum*, *L. tulipifera* and *Prunus serotina* were mostly found on north facing aspects (Desta et al., 2004). Topography also influences the degree of inter- and intra-crown shading and how shading varies with sun angle. Because tree species differ in their characteristic crown architecture, interactions between sun angle and crown shading throughout the growing season would be expected to vary between species. We applied a sun-canopy-sensor correction that was intended to remove the interactive effects of aspect, slope, and solar incidence angle on surface reflectance. Such techniques are not without criticism (i.e. they are simple geometric models of light interaction with topography), but the fact that we observed remaining influences of aspect supports the notion that topographic aspect influences greendown through vegetation type and crown architecture, which the sun-canopy-sensor correction is not designed to remove. It has been found that 30–50% of the variance in Landsat observations of VIS-red and NIR reflectance can be due to variation in inter- and intra-

Table 3
Model estimates for each vegetation association.

Vegetation type	Estimate						
	Model 1	Model 2	Model 3	Model 4	Model 6	Model 7	Model 8
Acer saccharum-Quercus rubra	0.0229.	0.0225.	0.0227.	0.0227.	0.0194	0.0149	−0.0019°
Cary sp.	0.0126	0.0171	0.0114	0.0141	0.0032	0.0076	0.0057°
Fraxinus americana-mix	0.0054	0.0049	0.0058	0.0054	−0.0079	−0.0020	−0.0015°
Pinus rigida	0.0088	0.0049	0.0070	0.0086	0.0042	0.0094	−0.0367*
Pinus strobus	0.0105	0.0091	0.0096	0.0116	0.0101	0.0076	−0.0312*
Pinus strobus-Quercus mix	0.0158	0.0141	0.0156	0.0153	0.0100	0.0156	−0.0077°
Pinus virginiana	0.0069	0.0033	0.0064	0.0073	0.0001	0.0026	−0.0569***
Pinus virginiana-deciduous mix	−0.0011	−0.0040	−0.0015	−0.0011	−0.0091	−0.0076	−0.0258*
Quercus alba	0.0285**	0.0267**	0.0279**	0.0280**	0.0215*	0.0254**	0.0081°
Quercus coccinea mix	0.0026	−0.0005	0.0001	0.0019	−0.0021	−0.0049	−0.0217.
Quercus prinus	−0.0012	−0.0006	−0.0002	−0.0012	−0.0070	−0.0136	−0.0150°
Quercus prinus -Acer rubrum mix	0.0140	0.0122	0.0181	0.0140	0.0153	−0.0013	0.0018°
Quercus prinus-Quercus coccinea	0.0017	0.0005	0.0029	0.0021	−0.0077	−0.0004	−0.0238.
Quercus prinus-Quercus mix	0.0042	0.0023	0.0038	0.0037	−0.0036	0.0000	−0.0117°
Quercus rubra	0.0185	0.0135	0.0208.	0.0185	0.0184	−0.0125	0.0025°
Quercus rubra-Quercus spp.- *Carya*	−0.0014	−0.0034	−0.0013	−0.0019	−0.0067	−0.0120	−0.0069°
Quercus velutina mix	−0.0040	−0.0082	−0.0044	−0.0051	−0.0089	−0.0182.	−0.0220.
Robinia pseudoacacia mix	0.0156	0.0127	0.0137	0.0162	0.0111	0.0079	−0.0007°
Tilia americana- Acer saccharum	0.0748*	0.0631*	0.0777*	0.0728*	0.0687*	0.0243	0.0469°
Tsuga canadensis	0.0164°	0.0176°	0.0180°	0.0172°	0.0172°	0.0180°	−0.0156°

p-value: 0 '***'; 0.001 '**'; 0.01 '*'; 0.05 '.'; 0.1 '°'. Model 5 excluded vegetation class and thus was excluded from this analysis.

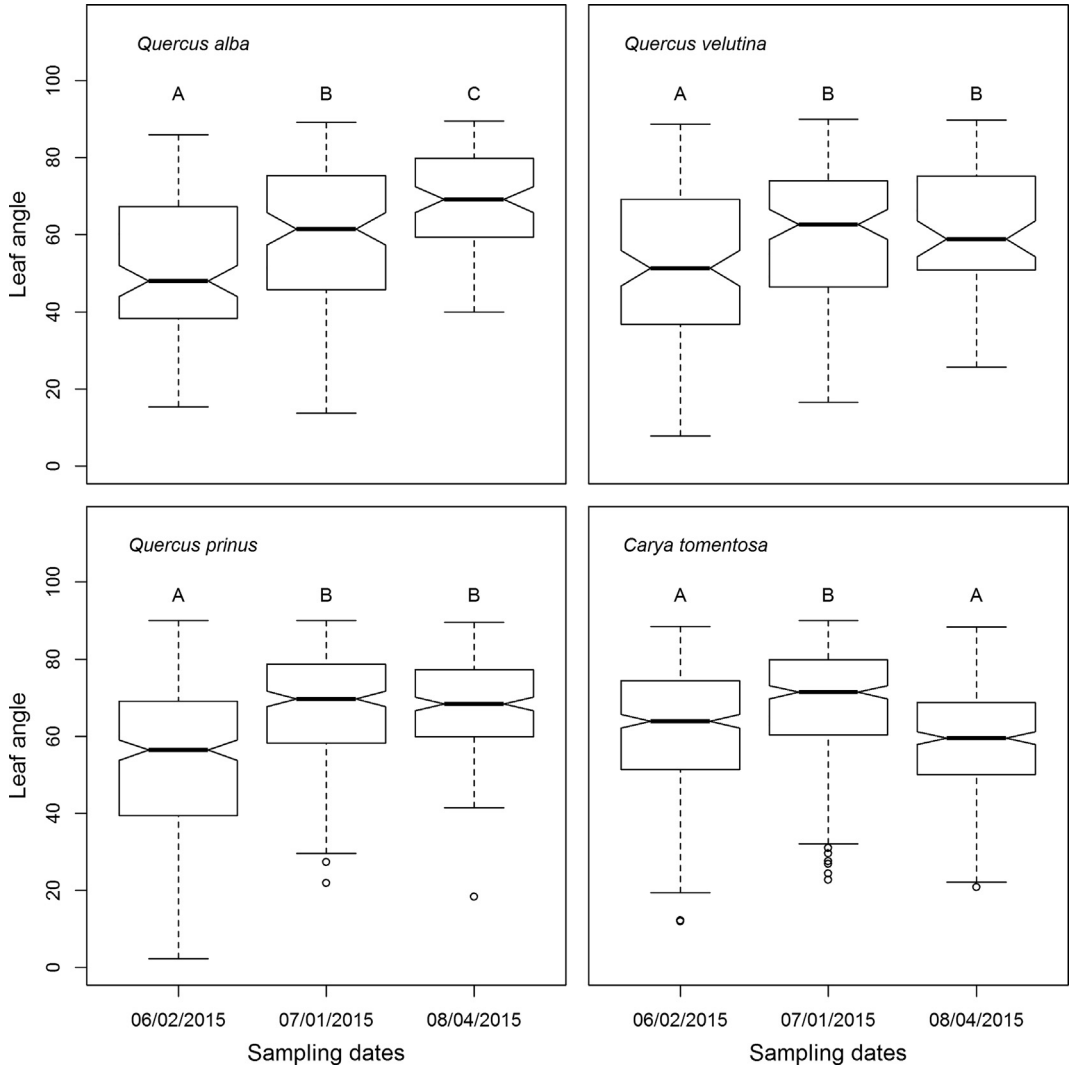

Fig. 3. Leaf angle data (relative to horizontal) taken from the visitor center overlook (*Q. alba*), and an old fire tower on Town Hill Mountain at Green Ridge State Forest (*Q. velutina*, *Q. prinus*, *C. tomentosa*).

Table 4
(A) *t*-test between June and August leaf variable means averaged to the site level. (B) correlation between Δ-leaf variable and greendown averaged to the site level. Bold indicates significant correlation ($p < 0.01$).

		Leaf variable					
		C	$\delta^{13}C$	N	VIS-red	NIR	NDVI
A	*t*-test	−0.8	1.4	0.78	**−7**	−0.49	**7.89**
	P-value	0.4	0.16	0.44	**< 0.01**	0.62	**< 0.01**
B	r^2	−0.11	−0.05	0.09	−0.13	−0.11	0.07
	P-value	0.15	0.33	0.18	0.11	0.15	0.25

crown shadowing (Asner, 1998). However, species-specific quantification of crown shadowing, and investigations for how these vary with lighting conditions throughout the growing season, have not been the focus of extensive research. But such work would be a logical next step to further understand the origin of greendown and motivates the measurement of tree crown-level variables described later.

The MaxVeg cover achieved in early summer (May–June) is a function of site productivity, which is itself dependent on topographic position and vegetation type. Therefore, the high explanatory power of MaxVeg (20–26% of model variance) also provides support for crown architectural influences on greendown. When MaxVeg was removed from the multiple regression model, R^2 values decreased from 0.47–0.50 to 0.43 (removing aspect also decreased R^2 to 0.43). However, MaxVeg and greendown are mathematically related in that high greendown requires high MaxVeg (greendown is the rate of decline in vegetation cover, which can only be high when vegetation cover begins at a large value). Therefore, care must be taken when evaluating the ecological significance of this result.

We were surprised that surface rugosity was only weakly related to greendown. Conceptually, effects of shadowing due to intra- and inter-crown architectural complexity (i.e. canopy complexity) within Landsat pixels should collectively influence greendown (Li and Strahler, 1992; Panferov et al., 2001; Sabol et al., 2002; Hardy et al., 2004; Asner et al., 2015). Radiative transfer models also suggest that increasing canopy complexity creates more shadows as the solar zenith angle increases throughout the growing season (Hall et al., 1995; Garcia-Haro and Sommer, 2002; Essery et al., 2008). Rugosity, defined here as the standard deviation of canopy height measured from LiDAR, showed spatial coherence with greendown, but across the 940 random locations we included in our multiple regression analysis, rugosity explained < 1% of the model variance. This suggests that even though rugosity has been shown to influence canopy shadowing in remote sensing images (i.e. (Parker and Russ, 2004; Ogunjemiyo et al., 2005)) other factors including aspect, elevation, and vegetation type overwhelm the effect of rugosity on greendown at this study area. Alternatively, our measure

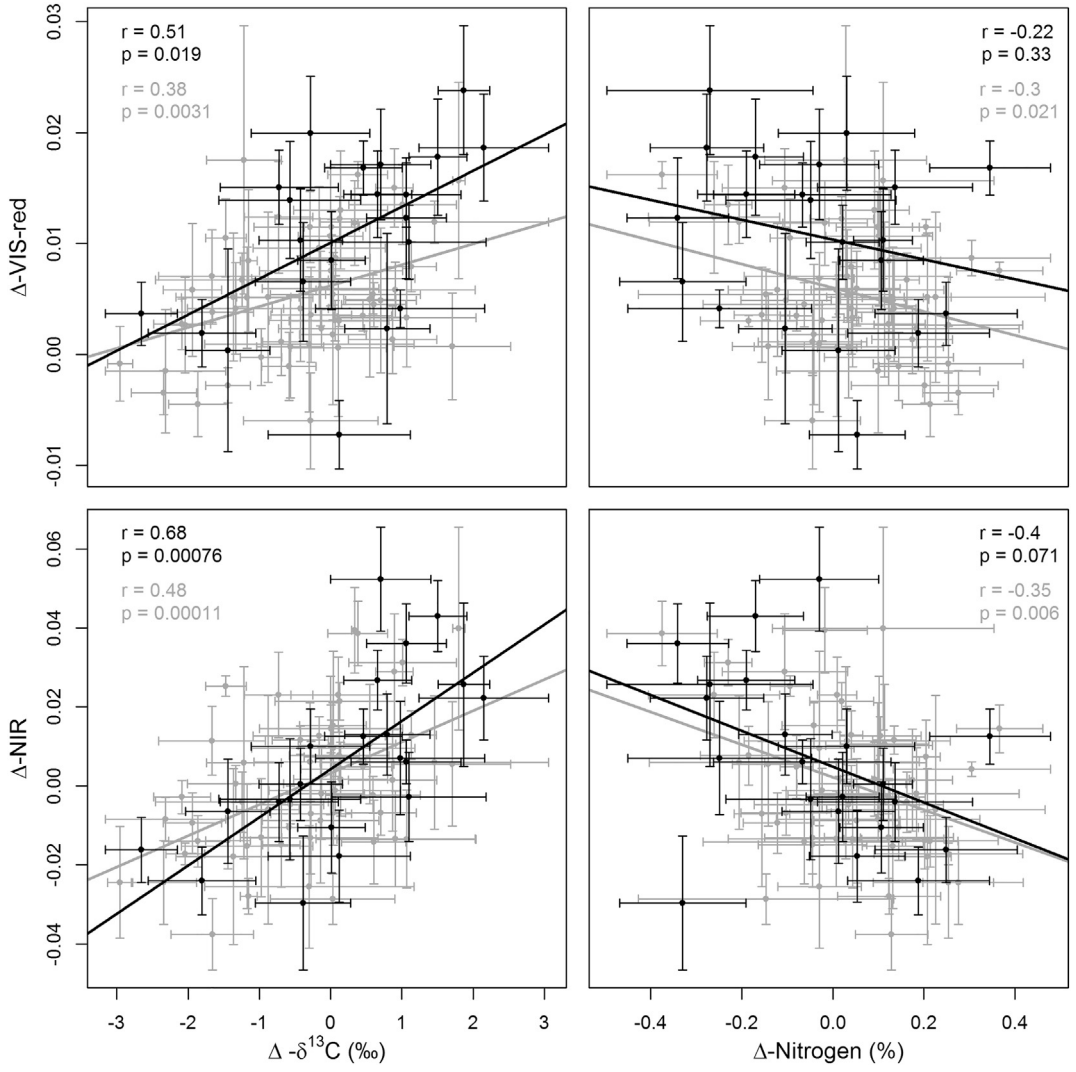

Fig. 4. Pearson correlation between foliar Δ-VIS-red and Δ-NIR with Δ-$\delta^{13}C$ and Δ-%N at the tree (gray) and site (black) levels of aggregation. Positive Δ values for $\delta^{13}C$ indicate that August was less negative (less discrimination against ^{13}C) compared to June. Error bars for Δ-leaf variable are the standard error for August and June added in quadrature.

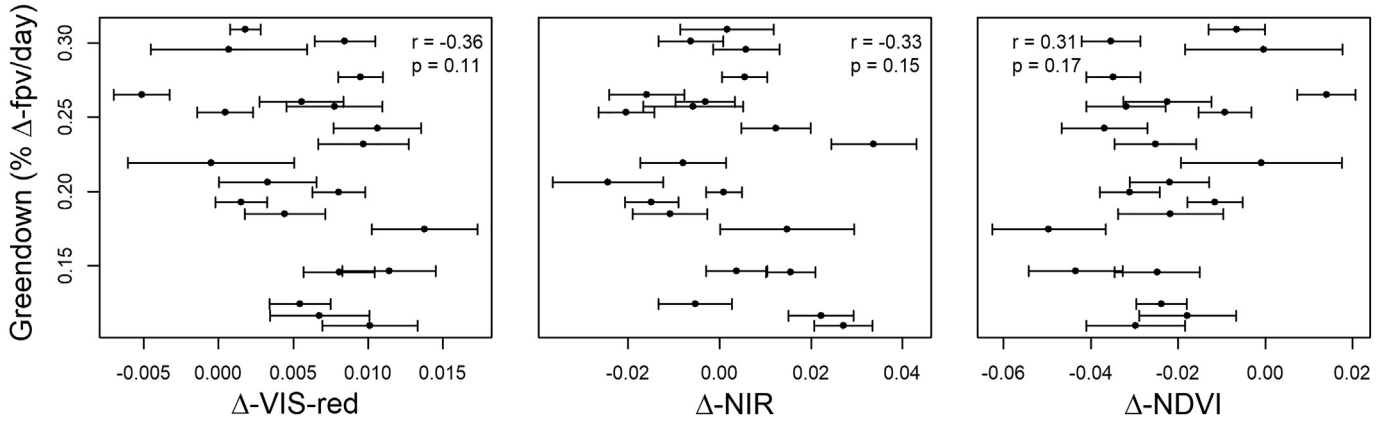

Fig. 5. Pearson correlation between greendown and change (Δ) in foliar reflectance and reflectance indices (VIS-red, NIR and NDVI) between June and August. Δ was calculated as the difference between August and June mean values for each site, therefore, positive Δ indicates the August value was higher than June value. Error bars for Δ-leaf variable are the standard error for August and June added in quadrature. Elmore et al. (2012) calculated 95% uncertainty intervals of ± 0.07% Δ f_{PV}/day for greendown, which would be identical for each measurement.

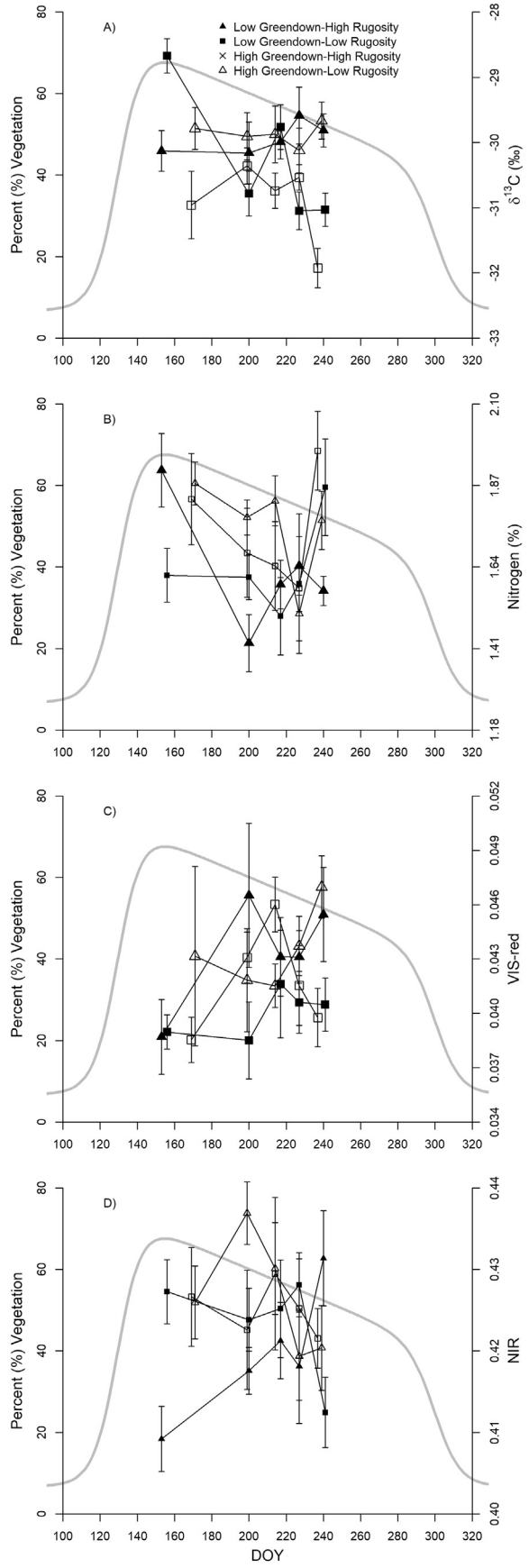

Fig. 6. Landsat phenology curves for four plots differing in greendown and canopy rugosity, superimposed with repeated *Q. alba* leaf measurements of (A) $\delta^{13}C$, (B) %N, (C) VIS- red reflectance, and (D) NIR reflectance.

of rugosity obtained from leaf-off LiDAR data with 1–4 returns per square meter could have been an inadequate description of canopy complexity and its theorized impact on greendown.

4.2. Tree crown-level variables

Leaf angle is one highly variable parameter of tree crown architecture that has a large influence on spectral reflectance, especially NIR reflectance (Asner, 1998), suggesting a contribution to landscape patterns of greendown. As leaf angle increases (more downward or upward pointing leaves) photons can travel farther into the canopy, increasing scattering, and through multiple interactions with plant parts, increase NIR attenuation and decrease NIR reflectance. Consistent with this understanding, we found that leaf angle increased throughout the growing season for three of the four species we measured (*Q. velutina*, *Q. prinus*, *Q. alba*,), and *Q. alba* exhibited the strongest trend. Given that *Q. alba* occurs at all of our sites, it is particularly relevant that this species showed the strongest evidence of increasing leaf angles. The two sites measured here are inadequate to draw strong conclusions, but these results do offer one more explanation for how inter-species variation in tree crown architecture could contribute to greendown and the observation that greendown is correlated with vegetation type.

4.3. Leaf-level variables

A key finding of our study is that variability in foliar reflectance and chemical traits was not spatially correlated with greendown. Thus, rather than being linked to a leaf-level mechanism, our results suggest that the degree of greendown in this oak-hickory forest is driven by mechanisms occurring at the landscape and tree crown levels. This might have been predicted from recent work comparing foliar chemical traits and reflectance with webcam observations of canopy greenness. Such work has emphasized the fact that canopy greenness from webcams peaks approximately 2 weeks earlier than foliar chlorophyll content (Keenan et al., 2014; Yang et al., 2014; Yang et al., 2016). Following peak greenness, a variety of growing season trends in foliar traits have been observed, including increasing carbon concentration, and increasing VIS-red and decreasing VIS-green reflectance (Keenan et al., 2014). However, these have not been mechanistically linked to greendown at the few sites analyzed. By measuring multiple sites across a gradient in greendown, we show more conclusively that growing season variation in leaf traits is not spatially correlated with greendown.

Nevertheless, our foliar reflectance and chemical data do exhibit important patterns that are consistent with an ecological interpretation of how traits and spectra can covary with site productivity and moisture stress. Our decision to sample the strongly anisohydric tree species of white oak (*Q. alba*) is likely consequential to our interpretations because this species maintains stomatal conductance even when water availability is low (Roman et al., 2015). Since discrimination against ^{13}C is greatest when stomatal conductance is highest, isotopic discrimination should be greatest at sites with high productivity. Indeed, we observed this effect as an increase in %N at sites with the largest increase in discrimination against ^{13}C. Therefore, observed seasonal changes in the leaf chemical traits of this anisohydric tree species revealed landscape variation in the ability of trees to maintain foliar %N, stomatal conductance, and likely productivity throughout the growing season.

The observed seasonal variation in leaf chemical traits correlated with variation in foliar NIR reflectance (both $\delta^{13}C$ and %N) and VIS-red reflectance ($\delta^{13}C$). For example, we observed that trees and sites with increasing %N and decreasing $\delta^{13}C$ (i.e., the most productive sites) exhibited declining foliar NIR reflectance throughout the growing season. Our research was not designed specifically to identify a mechanism for the observed decline in foliar NIR reflectance. However, these results suggest foliar structural changes (i.e., increased mesophyll

thickness) throughout the growing season that occur most strongly at locations exhibiting increasing %N and decreasing ^{13}C. We observed increased VIS-red reflectance at sites with the least discrimination against ^{13}C, supporting the idea that these sites represent the lowest rates of photosynthesis. If declining foliar NIR and increasing foliar VIS-red reflectance were to translate to changes in surface reflectance, we would expect increased greendown at these sites. However, we observed no correlations between foliar reflectance and greendown (Fig. 6). Therefore, we conclude that changes in foliar chemical traits and foliar reflectance did not translate to observable changes in surface reflectance that were spatially correlated with greendown.

5. Conclusions

We found that 50% of the spatial variability in greendown could be explained by landscape variables, with greendown particularly higher in locations with higher maximum greenness, more southerly aspects, or locations with greater abundance of white oak (*Quercus alba*). The importance of species composition as a driver of greendown was supported at the tree crown level, where, relative to three other tree species, we found the leaf angle of *Q. alba* to have the most consistent trend toward more vertical leaf angles later in the season. We observed declines in leaf-level spectral reflectance at some sites, but these were limited to locations where leaf %N and $\delta^{13}C$ data suggest high rates of productivity. Across all sites, leaf level spectral reflectance was not correlated with greendown. Collectively, our analysis from this oak-hickory forest indicates that growing season variation in the leaf-level observations made here, were overwhelmed by variation in the landscape and tree crown-level drivers of topography and species composition in controlling the spatial pattern of greendown. It is of course possible that we failed to measure the right leaf-level properties. Potential candidates for future work in this area might include leaf structural parameters (Gausman et al., 1971), the concentration of leaf pigments (Yang et al., 2014), or to include a measurement of a wider variety of tree species.

By comparing spatial factors correlated with greendown, our study highlights how this common feature of land surface phenology datasets can be productively used to help unravel the relative importance of leaf-, tree crown-, and landscape-level drivers of spectral reflectance. Just as leaf-level drivers appear to be more important in the more productive locations of our oak-hickory forest study area, the relative importance of these drivers is likely to differ in other contexts. Similarly, just as species differences in our tree crown-level leaf angle observations could be readily interpreted alongside the landscape-level finding of the importance of species composition, analyzing variability in greendown can also help elucidate or confirm how mechanisms may interact across scales. Ultimately, insights into the drivers of surface reflectance will be essential for improving our ability to translate land surface phenology data into predictions of ecosystem structure and functioning.

Acknowledgments

We would like to thank Steven Guinn, Ian Smith, Robin Paulman, Regina Trott, Kavya Pradhan, Susan Snow and Larry Reaves for their technical assistance. This research was funded by NASA, grant NNX12AK17G. B.E.M. is grateful for Research Initiation Grant funding from the NASA WV EPSCoR/Space Grant Consortium, the Harvard Forest Bullard Fellowship program, and the WVU Student Undergraduate Research Experience Fellowships that helped fund the leaf angle analysis completed by Evelin Flamenco, Christopher King, and Samual Rescorl.

Appendix A. Supplementary data

Supplementary data associated with this article can be found in the online version, at https://doi.org/10.1016/j.rse.2018.03.027. These data include the Google map of the most important areas described in this article.

References

Adams, J.B., Smith, M.O., Johnson, P.E., 1986. Spectral mixture modeling: a new analysis of rock and soil types at the Viking Lander 1 Site. J. Geophys. Res. Solid Earth Planets 91 (B8), 8098–8112.
Asner, G.P., 1998. Biophysical and biochemical sources of variability in canopy reflectance. Remote Sens. Environ. 64 (3), 234–253.
Asner, G.P., Warner, A.S., 2003. Canopy shadow in IKONOS satellite observations of tropical forests and savannas. Remote Sens. Environ. 87 (4), 521–533.
Asner, G.P., Martin, R.E., Anderson, C.B., Knapp, D.E., 2015. Quantifying forest canopy traits: imaging spectroscopy versus field survey. Remote Sens. Environ. 158, 15–27.
Badgley, G., Field, C.B., Berry, J.A., 2017. Canopy near-infrared reflectance and terrestrial photosynthesis. Sci. Adv. 3 (3), e1602244.
Bassow, S., Bazzaz, F., 1998. How environmental conditions affect canopy leaf-level photosythensis in four dedicduous tree species. Ecology 79 (8), 2660–2675.
Choat, B., Jansen, S., Brodribb, T.J., Cochard, H., Delzon, S., Bhaskar, R., Bucci, S.J., Feild, T.S., Gleason, S.M., Hacke, U.G., 2012. Global convergence in the vulnerability of forests to drought. Nature 491 (7426), 752–755.
Desta, F., Colbert, J.J., Rentch, J.S., Gottschalk, K.W., 2004. Aspect induced differences in vegetation, soil, and microclimatic characteristics of an Appalachian watershed. Castanea 69 (2), 92–108.
Dragoni, D., Rahman, A.F., 2012. Trends in fall phenology across the deciduous forests of the Eastern USA. Agric. For. Meteorol. 157, 96–105.
Elmore, A.J., Mustard, J.F., Manning, S.J., Lobell, D.B., 2000. Quantifying vegetation change in semiarid environments: precision and accuracy of spectral mixture analysis and the Normalized Difference Vegetation Index. Remote Sens. Environ. 73 (1), 87–102.
Elmore, A.J., Guinn, S.M., Minsley, B.J., Richardson, A.D., 2012. Landscape controls on the timing of spring, autumn, and growing season length in mid-Atlantic forests. Glob. Chang. Biol. 18 (2), 656–674.
Essery, R., Bunting, P., Hardy, J., Link, T., Marks, D., Melloh, R., Pomeroy, J., Rowlands, A., Rutter, N., 2008. Radiative transfer modeling of a coniferous canopy characterized by airborne remote sensing. J. Hydrometeorol. 9 (2), 228–241.
Farquharson, C.G., Oldenburg, D.W., 1998. Non-linear inversion using general measures of data misfit and model structure. Geophys. J. Int. 134 (1), 213–227.
Fisher, J.I., Mustard, J.F., Vadeboncoeur, M.A., 2006. Green leaf phenology at Landsat resolution: scaling from the field to the satellite. Remote Sens. Environ. 100 (2), 265–279.
Foster, J.R., Townsend, P.A., 2004. Linking hyperspectral imagery and forest inventories for forest assessment in the Central Appalachians. In: Proceedings of the 14th Central Hardwood Conference.
Garcia-Haro, F.J., Sommer, S., 2002. A fast canopy reflectance model to simulate realistic remote sensing scenarios. Remote Sens. Environ. 81 (2–3), 205–227.
Gausman, H., Allen, W., Escobar, D., Rodriquez, R., Cardenas, R., 1971. Age effects of cotton leaves on light reflectance, transmittance, and absorptance and on water content and thickness. Agron. J. 63 (3), 465–469.
Gu, D., Gillespie, A., 1998. Topographic normalization of landsat TM images of forest based on subpixel Sun-canopy-sensor geometry. Remote Sens. Environ. 64 (2), 166–175.
Hall, F.G., Shimabukuro, Y.E., Huemmrich, K.F., 1995. Remote sensing of forest biophysical structure using mixture decomposition and geometric reflectance models. Ecol. Appl. 5 (4), 993–1013.
Hardy, J.P., Melloh, R., Koenig, G., Marks, D., Winstral, A., Pomeroy, J.W., Link, T., 2004. Solar radiation transmission through conifer canopies. Agric. For. Meteorol. 126 (3–4), 257–270.
Hwang, T., Song, C.H., Bolstad, P.V., Band, L.E., 2011. Downscaling real-time vegetation dynamics by fusing multi-temporal MODIS and Landsat NDVI in topographically complex terrain. Remote Sens. Environ. 115 (10), 2499–2512.
Hwang, T., Band, L.E., Miniat, C.F., Song, C.H., Bolstad, P.V., Vose, J.M., Love, J.P., 2014. Divergent phenological response to hydroclimate variability in forested mountain watersheds. Glob. Chang. Biol. 20 (8), 2580–2595.
Jennings, M.D., Faber-Langendoen, D., Loucks, O.L., Peet, R.K., Roberts, D., 2009. Standards for associations and alliances of the US National Vegetation Classification. Ecol. Monogr. 79 (2), 173–199.
Keenan, T.F., Darby, B., Felts, E., Sonnentag, O., Friedl, M.A., Hufkens, K., O'Keefe, J., Klosterman, S., Munger, J.W., Toomey, M., Richardson, A.D., 2014. Tracking forest phenology and seasonal physiology using digital repeat photography: a critical assessment. Ecol. Appl. 24 (6), 1478–1489.
Li, X.W., Strahler, A.H., 1992. Geometric optical bidirectional reflectance modeling of the discrete crown vegetation canopy, effect of crown shape and mutual shadowing. IEEE Trans. Geosci. Remote Sens. 30 (2), 276–292.
Masek, J.G., Vermote, E.F., Saleous, N.E., Wolfe, R., Hall, F.G., Huemmrich, K.F., Gao, F., Kutler, J., Lim, T.K., 2006. A Landsat surface reflectance dataset for North America, 1990–2000. IEEE Geosci. Remote Sens. Lett. 3 (1), 68–72.
Melaas, E., Friedl, M., Zhu, Z., 2012. Monitoring Interannual Variation in Deciduous Broadleaf Forest Phenology Using Landsat. AGU Fall Meeting Abstracts.
Melaas, E.K., Friedl, M.A., Zhu, Z., 2013. Detecting interannual variation in deciduous broadleaf forest phenology using Landsat TM/ETM plus data. Remote Sens. Environ. 132, 176–185.
Melaas, E.K., Sulla-Menashe, D., Gray, J.M., Black, T.A., Morin, T.H., Richardson, A.D.,

Friedl, M.A., 2016. Multisite analysis of land surface phenology in North American temperate and boreal deciduous forests from Landsat. Remote Sens. Environ. 186, 452–464.
Ogunjemiyo, S., Parker, G., Roberts, D., 2005. Reflections in bumpy terrain: implications of canopy surface variations for the radiation balance of vegetation. IEEE Geosci. Remote Sens. Lett. 2 (1), 90–93.
Ollinger, S.V., 2011. Sources of variability in canopy reflectance and the convergent properties of plants. New Phytol. 189 (2), 375–394.
Owenby, J.R., Ezell, D.S., 1992. Monthly Station Normals of Temperature, Precipitation, Heating and Cooling Degree Days 1961–1990 Climatography of the United States No. 81. National Climatic Data Center, Asheville, NC, U.S. Department of Commerce, National Oceanic and Atmospheric Administration, pp. 18.
Panferov, O., Knyazikhin, Y., Myneni, R.B., Szarzynski, J., Engwald, S., Schnitzler, K.G., Gravenhorst, G., 2001. The role of canopy structure in the spectral variation of transmission and absorption of solar radiation in vegetation canopies. IEEE Trans. Geosci. Remote Sens. 39 (2), 241–253.
Parker, G.G., Russ, M.E., 2004. The canopy surface and stand development: assessing forest canopy structure and complexity with near-surface altimetry. For. Ecol. Manag. 189 (1–3), 307–315.
Perry, D.A., 1994. Forest Ecosystems. JHU Press.
Pisek, J., Ryu, Y., Alikas, K., 2011. Estimating leaf inclination and G-function from leveled digital camera photography in broadleaf canopies. Trees 25 (5), 919–924.
Pisek, J., Sonnentag, O., Richardson, A.D., Mõttus, M., 2013. Is the spherical leaf inclination angle distribution a valid assumption for temperate and boreal broadleaf tree species? Agric. For. Meteorol. 169, 186–194.
Raabe, K., Pisek, J., Sonnentag, O., Annuk, K., 2015. Variations of leaf inclination angle distribution with height over the growing season and light exposure for eight broadleaf tree species. Agric. For. Meteorol. 214, 2–11.
Reich, P.B., Walters, M.B., Ellsworth, D.S., 1991. Leaf age and season influence the relationships between leaf nitrogen, leaf mass perarea and photosynthesis in maple and oak trees. Plant Cell Environ. 14 (3), 251–259.
Roman, D., Novick, K., Brzostek, E., Dragoni, D., Rahman, F., Phillips, R., 2015. The role of isohydric and anisohydric species in determining ecosystem-scale response to severe drought. Oecologia 179 (3), 641.
Ryu, Y., Sonnentag, O., Nilson, T., Vargas, R., Kobayashi, H., Wenk, R., Baldocchi, D.D., 2010. How to quantify tree leaf area index in an open savanna ecosystem: a multi-instrument and multi-model approach. Agric. For. Meteorol. 150 (1), 63–76.
Sabol, D.E., Gillespie, A.R., Adams, J.B., Smith, M.O., Tucker, C.J., 2002. Structural stage in Pacific Northwest forests estimated using simple mixing models of multispectral images. Remote Sens. Environ. 80 (1), 1–16.
Scales, J.A., Gersztenkorn, A., Treitel, S., 1988. Fast Ip solution of large, sparse, linear systems: application to seismic travel time tomography. J. Comput. Phys. 75 (2), 314–333.
Small, C., 2004. The Landsat ETM+ spectral mixing space. Remote Sens. Environ. 93, 1): 1–17.
Smith, M.O., Ustin, S.L., Adams, J.B., Gillespie, A.R., 1990. Vegetation in deserts. 1. A regional measure of abundance from multispectral images. Remote Sens. Environ. 31 (1), 1–26.
Tucker, C.J., 1979. Red and photographic infrared linear combinations for monitoring vegetation. Remote Sens. Environ. 8 (2), 127–150.
Wilson, K.B., Baldocchi, D.D., Hanson, P.J., 2000. Spatial and seasonal variability of photosynthetic parameters and their relationship to leaf nitrogen in a deciduous forest. Tree Physiol. 20 (9), 565–578.
Woodcock, C.E., Allen, R., Anderson, M., Belward, A., Bindschadler, R., Cohen, W., Gao, F., Goward, S.N., Helder, D., Helmer, E., 2008. Free access to Landsat imagery. Science 320 (5879) (1011-1011).
Yang, X., Tang, J.W., Mustard, J.F., 2014. Beyond leaf color: comparing camera-based phenological metrics with leaf biochemical, biophysical, and spectral properties throughout the growing season of a temperate deciduous forest. Journal of Geophysical Research-Biogeosciences 119 (3), 181–191.
Yang, X., Tang, J., Mustard, J.F., Wu, J., Zhao, K., Serbin, S., Lee, J.-E., 2016. Seasonal variability of multiple leaf traits captured by leaf spectroscopy at two temperate deciduous forests. Remote Sens. Environ. 179, 1–12.
Zhang, X.Y., Friedl, M.A., Schaaf, C.B., Strahler, A.H., Hodges, J.C.F., Gao, F., Reed, B.C., Huete, A., 2003. Monitoring vegetation phenology using MODIS. Remote Sens. Environ. 84 (3), 471–475.
Zhang, X., Friedl, M.A., Schaaf, C.B., Strahler, A.H., 2004. Climate controls on vegetation phenological patterns in northern mid-and high latitudes inferred from MODIS data. Glob. Chang. Biol. 10 (7), 1133–1145.
Zhu, Z., Woodcock, C.E., 2012. Object-based cloud and cloud shadow detection in Landsat imagery. Remote Sens. Environ. 118, 83–94.
Zhu, Z., Woodcock, C.E., 2014. Continuous change detection and classification of land cover using all available Landsat data. Remote Sens. Environ. 144, 152–171.